Water vapor absorption continuum under nonequilibrium vibrational conditions

O.G. Buzykin and S.V. Ivanov

N.E. Zhukovskii Central Aerohydrodynamic Institute, Zhukovskii
Institute for Problems of Laser and Information Technologies, Russian Academy of Sciences, Troitsk

Received December 27, 2002

The formulation of water vapor continuum absorption under non-LTE vibrational conditions is presented. The semi-empirical approach of Clough, Kneizys and Davies is extended to non-LTE vibrational conditions assuming rotational-translational LTE. Self- and air-broadened $H_2{}^{16}O$ continuum is simulated in 0–5500 cm^{-1} spectral region at the constant temperature T = 288 K. The possibility of marked nonequilibrium bleaching of continuum in certain spectral regions is demonstrated and explained by full and partial population inversion effects between H_2O energy levels. The absorption increase in some other regions is also obtained. A more flexible method of continuum characterization is proposed based on the use of several semi-empirical χ-functions for H_2O line shapes, which should be determined separately for each band using experimental data. Possible experiments revealing the nature of water vapor absorption continuum (monomer / dimer) are discussed based on the theoretical results obtained.

Introduction

Water vapor absorption continuum contributes considerably to optical characteristics of the atmosphere in many spectral regions. In spite of numerous publications (see, for example, bibliography on www.watervaporcontinuum.com), the nature of water vapor absorption continuum is not still completely clear. It is a common practice to explain water vapor absorption in atmospheric windows by the following hypotheses: contribution of far wings of strong rotation-vibration lines of the water monomer Í2Î (Refs. 1–6); radiation absorption in rotation-vibration bands of the water dimer $(Í_2Î)_2$ and collision-induced absorption (Refs. 7–12); nonlinear phenomena (Refs. 13 and 14). One more hypothesis concerned the possible role of water ion clusters.[15,16] Under field conditions, the above factors are complemented with aerosol extinction,[17,18] which is very hard to monitor.

The most well-known and widely used semiempirical CKD model of water vapor continuum for the clean (without aerosol) atmosphere was developed by Clough, Kneizys, and Davies in 1989 (Ref. 3). Their approach provides for a uniform description of the absorption continuum in a wide spectral region from the microwaves to the near IR. This is a remarkable advantage of the CKD model over other empirical models that are good only for relatively narrow spectral ranges (see, for example, Refs. 9 and 19). The CKD model is based on the monomer hypothesis on the nature of water continuum and can be used only under equilibrium conditions. As we know, by now all experimental investigations of water vapor continuum were conducted under conditions of local thermodynamic equilibrium (LTE), and no attempts have yet been made to construct non-LTE models of water vapor continuum.

At the same time, it is known that nonequilibrium effects are observed in some practical applications connected with remote sensing of the atmosphere and in many laboratory investigations. The following phenomena give rise to different kinds of nonequilibrium in air: electric discharges, particle beam propagation, chemical and photochemical reactions, exposure of molecules to laser radiation, super- and hypersonic gas flows, etc. (see, for example, Refs. 20–25). Nonequilibrium conditions are usually divided into electronic, vibrational, and rotational. This division is based, essentially, on different "temperature" of population of energy levels (electronic, vibrational, rotational) and kinetic (translational) temperature.[20] In the case of vibrational nonequilibrium $T_V \neq T_R = T$. Rotational degrees of freedom having the temperature T_R are believed here to be in equilibrium with the translational degrees of freedom characterized by the temperature T. The vibrational temperature T_V for a two-level system is determined as

$$T_V = (E_{V_1} - E_{V_0}) \Big/ k_B \ln\left(\frac{N_0}{N_1}\frac{g_{V_1}}{g_{V_0}}\right),$$

where N_0, N_1 and g_{V_0}, g_{V_1} are the populations and statistical weights of the vibrational levels |0> and |1>; k_B is the Boltzmann constant.[25]

The most significant non-LTE effects arise at population inversion of energy levels: full (vibrational) and partial (rotation-vibration) ones. The population inversion manifests itself in spectra as an increase of absorption at some transitions and a decrease at others till appearance of negative

absorption (amplification).[26–28] A classical example of this effect in water vapor is the water-vapor laser,[29] in which electric discharge initiates inversion between the lower levels of the H_2O ν_1 and ν_3 modes and the lower levels of the ν_2 mode. Lasing was obtained experimentally at many pure rotational transitions in H_2O (thanks to rotational population inversion) belonging to the states (100), (001), (010), and (020), as well as rovibrational transitions (thanks to the full and partial inversion) in the (100)–(020), (001)–(020), and (020)–(010) bands.

The aim of this work is the following: 1) to develop a model of water vapor continuum absorption for non-LTE vibrational conditions and to study the most significant effects; 2) to propose a method for improving the description of continuum by means of semiempirical χ-functions for line profiles of the water monomer; 3) to propose experiments opening new possibilities in studying the nature of water vapor continuum and based on investigation of the Í 2 Î absorption spectrum under non-LTE conditions.

1. Main equations

1.1. Equilibrium CKD model

The classical equilibrium CKD technique[3] is based on the assumption that water vapor continuum is formed by far wings of strong absorption lines of the water monomer Í 2 Î. The main attention is paid to choosing the profiles of spectral lines at large distances from line centers in such a way that the calculated spectrum to coincide with the experimental one both in pure water vapor and in air including water vapor as a minor gas. The following equation for the absorption coefficient (cm^2/mol) that is suitable both in the infrared and in the microwave regions is used[3]:

$$\alpha(\nu) = R(\nu,T)\sum_i \tilde{S}_i \frac{1}{\pi}\left[\frac{\gamma_i}{(\nu-\nu_i)^2+\gamma_i^2}\chi(\nu_i-\nu) + \frac{\gamma_i}{(\nu+\nu_i)^2+\gamma_i^2}\chi(\nu_i+\nu)\right]. \quad (1)$$

Here $R(\nu, T) = \nu \tanh(\beta\nu/2)$, $\beta = hc/k_BT$; $\tilde{S}_i = S_i/R(\nu_i, T)$; ν is wavenumber, cm^{-1}; T is gas temperature; c is the speed of light; h and k_B are, respectively, the Planck's and Boltzmann constants; S_i, ν_i, γ_i are the integral intensity, cm^2/mol, line position, and collisional half-width of the ith absorption line. The semiempirical function χ describes deviation of the actual spectral line profile from the Lorentz one and is used to fit calculations to the experimental data. Continuum is a slowly varying part of the actual absorption spectrum. It is described by the following equation:

$$\alpha_c(\nu) = R(\nu,T)[\tilde{C}_s^0(N_s/N_0) + \tilde{C}_f^0(N_f/N_0)], \quad (2)$$

where $\tilde{C}_s^0$ and $\tilde{C}_f^0$ are the coefficients responsible for self-broadening and buffer gas pressure induced broadening; N_s, N_f, and N_0 are the corresponding number densities (subscripts f, s, and 0 stand for respectively the buffer gas (dry air), active gas (water vapor), and atmospheric air). Here α_c is also measured in cm^2/mol. The continuum coefficients $\tilde{C}_s^0$ and $\tilde{C}_f^0$ (they are measured in cm^3/mol) are calculated as follows:

$$\tilde{C}_\mu^0(\nu)(N_\mu/N_0) = \sum_i \tilde{S}_i[f_c(\nu-\nu_i)\chi(\nu-\nu_i) + f_c(\nu+\nu_i)\chi(\nu+\nu_i)], \quad (3)$$

where $\mu = s$, f; the function $f_c(\nu \mp \nu_i)$ is the line profile with the strong central part excluded. It has the following form:

$$f_c(\nu \mp \nu_i) = \begin{cases} \dfrac{1}{\pi}\dfrac{\gamma_i}{25^2+\gamma_i^2}, & |\nu \mp \nu_i| \le 25\ cm^{-1}, \\ \dfrac{1}{\pi}\dfrac{\gamma_i}{(\nu \mp \nu_i)^2+\gamma_i^2}, & |\nu \mp \nu_i| \ge 25\ cm^{-1}. \end{cases}$$

In Ref. 3 the χ-function was presented as:

$$\chi = \begin{cases} 1-(1-\chi')\dfrac{(\nu \mp \nu_i)^2}{25^2}, & |\nu \mp \nu_i| \le 25\ cm^{-1}, \\ \chi', & |\nu \mp \nu_i| \ge 25\ cm^{-1}. \end{cases} \quad (4)$$

In the case of self-broadening the function χ' has the form

$$\chi' = \chi'_s = 8.63\exp(-z_1^2) + (0.83z_2^2 + 0.033z_2^4)\exp(-|z_2|).$$

The functions z_1 and z_2 at T = 296 K are defined as $z_1 = (\nu \mp \nu_i)/400$, $z_2 = (\nu \mp \nu_i)/250$. In the case of buffer gas (air) pressure induced broadening

$$\chi' = \chi'_f = 6.65\exp(-z_1^2),\ z_1 = (\nu \mp \nu_i)/75.$$

In Ref. 3 the parameters of the χ-function were obtained by the least squares fitting of the calculated continuum spectrum to Burch's experimental data.[30–32]

1.2. Extension to non-LTE conditions

The idea of our approach consist in separate consideration of the effects of variation in population of H_2O levels and change of the gas temperature when developing the model of continuum. In this paper we restricted our consideration to simulation of only vibrational nonequilibrium of H_2O at the balance translational and rotational degrees of freedom ($T_V \neq T_R = T$ = const). The entire water vapor continuum in the region from zero to 5500 cm^{-1} was divided into contributions coming from individual absorption bands, which depended on the population of vibrational levels.

The integral intensity S_{ik} of a rovibrational (RV) absorption line i in the band k corresponding to the transition $L_k \to U_k$ between the lower L_k and upper U_k vibrational levels can be written as follows[20,28]:

$$S_{ik} = \tilde{S}_{ik} R(\nu_{ik}, T) = \frac{c^2 A_{ik}}{8\pi\nu_{ik}^2} \left(N_{L_k} q_{R_{L_{ik}}} \frac{g_{U_{ik}}}{g_{L_{ik}}} - N_{U_k} q_{R_{U_{ik}}} \right), \quad (5)$$

where $q_{R_{L_{ik}}}$ and $q_{R_{U_{ik}}}$ are equilibrium rotational distribution functions for the states L_k and U_k; $g_{L_{ik}}$ and $g_{U_{ik}}$ are the statistical weights of the lower and upper RV levels; A_{ik} is the first Einstein coefficient for the RV transition under consideration. The coefficient of continuous absorption $\alpha_c(\nu)$ (cm^{-1}) at this frequency is determined by the sum of contributions from all the bands:

$$\alpha_c(\nu) = R(\nu, T) \times$$

$$\times \sum_k [(\tilde{C}^0_{sL_k} P_s + \tilde{C}^0_{fL_k} P_f) N_{L_k} - (\tilde{C}^0_{sU_k} P_s + \tilde{C}^0_{fU_k} P_f) N_{U_k}] , \quad (6)$$

$$\tilde{C}^0_{L_k}(\nu) P_\mu = \sum_i \frac{c^2 A_{ik}}{8\pi\nu_{ik}^2 R(\nu_{ik}, T)} q_{R_{L_{ik}}} \times$$

$$\times \frac{g_{U_{ik}}}{g_{L_{ik}}} [f_c(\nu - \nu_{ik}) \chi_k(\nu - \nu_{ik}) + f_c(\nu + \nu_{ik}) \chi_k(\nu + \nu_{ik})] \infty ,$$

$$\tilde{C}^0_{U_k}(\nu) P_\mu = \sum_i \frac{c^2 A_{ik}}{8\pi\nu_{ik}^2 R(\nu_{ik}, T)} q_{R_{U\,ik}} \times$$

$$\times [f_c(\nu - \nu_{ik}) \chi_k(\nu - \nu_{ik}) + f_c(\nu + \nu_{ik}) \chi_k(\nu + \nu_{ik})] ,$$

$$\gamma_i(P, T) = \gamma_s^0 P_s \left(\frac{296}{T} \right)^{n_s} + \gamma_f^0 P_f \left(\frac{296}{T} \right)^{n_f} .$$

Here P_μ is the partial pressure ($\mu = s, f$, i.e., P_s or P_f). In these equations, we used a more common representation of continuum through pressures, rather than number densities, which coincides with the representation from Ref. 3 at a constant temperature. In equation for the line halfwidth, γ_s^0 and γ_f^0 are the H_2O self-broadening coefficient (at 1 atm and 296 K) and the coefficient of buffer gas pressure induced broadening ($cm^{-1} \cdot atm^{-1}$); n_s and n_f are the exponents of the temperature dependence of the line width for these cases.

2. Results of numerical simulation

The calculations performed used the HITRAN-96 database[33] for the temperature T = 288 K corresponding to the temperature of the standard atmosphere at the zero height, as well as in some cases for T = 296 K. Only the main isotopic species $H_2{}^{16}O$ was considered. Since the data on self-broadening for many lines are absent from HITRAN-96, we assumed that $\gamma_s^0 = 5\gamma_f^0$ and $n_s = n_f$ for all lines. As the first step, χ-functions were believed identical for all Í$_2$Î bands, and their parameters were taken the same as in the initial CKD model (see Eq. (4)). Since the data for parameters of the χ-function at the temperature of 288 K were lacking, in calculations we used the parameters for 296 K.

When calculating absorption, we took into account all H_2O transitions in the region of 0–5500 cm^{-1} that are included in HITRAN-96 (5 purely rotational and 20 rovibrational bands involving 11 vibrational levels). The H_2O vibrational levels and transitions taken into account are shown in Fig. 1.

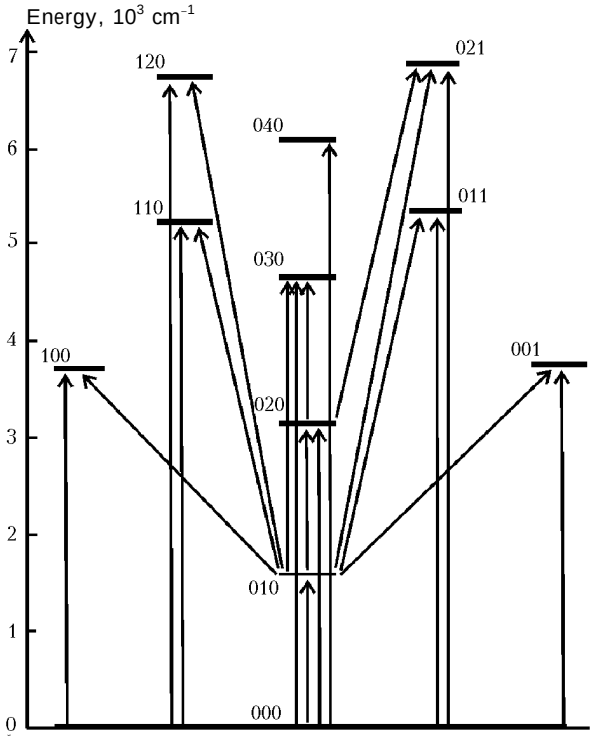

Fig. 1. Vibrational levels of the H_2O molecule and transitions taken into account in the spectroscopic scheme.

In simulating, we took into consideration the possibility of collisional relaxation of the selected vibrational states. The model of vibrational kinetics[26,27,34] includes rate equations for 11 levels of H_2O, N_2, and O_2 with the allowance for the VV-, VV′-, and VT-processes of collisional exchange. The H_2O, N_2, and O_2 levels and transitions are shown in Fig. 2.

The absorption spectrum was calculated with a rather small frequency step (2 cm^{-1}). Logarithms of the coefficients $\tilde{C}^0_k$ for every band were approximated by means of smoothing splines, whose parameters and coefficients were saved in data arrays. These arrays were then used in the main program, which calculated the coefficient of continuous absorption under given conditions. To decrease the bulk of data, spectral smoothing of small-scale pulsations arising in the calculated spectrum of continuum was performed. These pulsations are not connected with the physics of the phenomenon, but

rather with the form of the χ-function used. The presence of no more than two maxima was allowed in the vicinity of the center of each absorption band.

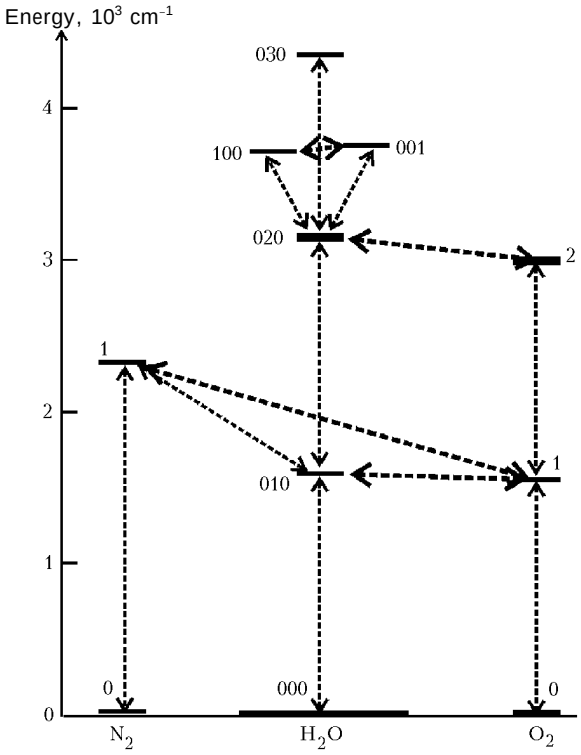

Fig. 2. Vibrational levels of H_2O, N_2, and O_2 and transitions taken into account in the scheme of relaxation kinetics.

For the case of broadening by buffer gases (air), the CKD method gives significantly lower absorption in the atmospheric windows in the region of 1000 and 2500 cm^{-1} as compared to the experimental data by Roberts et al.[9] In Ref. 3 this fact is explained by other absorption mechanisms (collision-induced spectra, humidity-dependent aerosol absorption), and it is proposed to take them into account through addition of a fitting constant into the equation for α_c (unfortunately, this constant was not presented in Ref. 3). Our calculation showed that rather good agreement of the functions with $\tilde{C}_f(\nu)$ [Fig. 6 in Ref. 3] is achieved, if we add the constant $0.75 \cdot 10^{-26}\, N_s \nu^{-1/2} \times R(\nu, T)$ cm^{-1} to α_c (here N_s is the number density of water vapor, cm^{-3}).

2.1. Test for equilibrium conditions and comparison with other data

To test the proposed technique, we first calculated a particular case of equilibrium continuum. Figure 3 demonstrates the contribution of individual bands to continuum absorption of the equilibrium atmosphere. Comparison of our calculations for equilibrium with some available results is shown in Fig. 4 (continuum at self-broadening) and Fig. 5 (continuum at broadening by air pressure). These figures reflect the current state of information about the water vapor continuum.

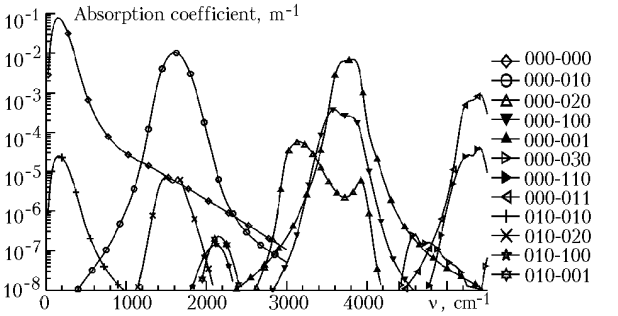

Fig. 3. Contribution of individual H_2O bands to the equilibrium absorption. Standard atmosphere: P = 1 atm, $\dot{O}$ = 288 K, $\tilde{N}_{H_2O}$ = $7.75 \cdot 10^3$ ppmV.

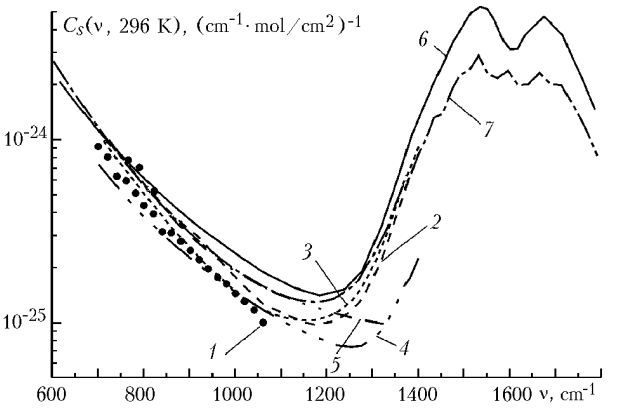

Fig. 4. Current state of the data on water vapor continuum at self-broadening: Burch's experiment[30–32] (*1*); CKD_2.2 (1996) model (*2*); CKD_0 (1989) model (*3*); Ma and Tipping calculation (1992) (*4*); Roberts et al. measurements[9] (1976) (*5*); Clough et al. calculation[3] (1989) (*6*); our calculation (*7*). The data *1–5* are borrowed from www.aer.com.

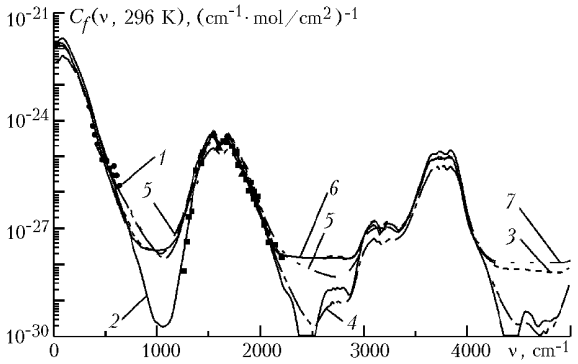

Fig. 5. Current state of data on water vapor continuum at air pressure induced broadening: Burch's experiment[30–32] for 296 K (circles), 308 K (triangles), and 353 K (squares) (*1*); CKD_2.2 (1996) model (*2*); CKD_0 (1989) model (*3*); Ma and Tipping (1992) (*4*); Thomas model[19] (1995) (*5*); Clough et al. calculation[3] (*6*); our calculation (*7*). The data *1–4* are borrowed from www.aer.com.

From Figs. 4 and 5 we can draw the following conclusions: (1) there exists a significant scatter in the

available data for both self-broadening of H_2O and air pressure induced broadening; (2) our results fall within this scatter and are in a good agreement with the results of Ref. 3; (3) H_2O continuum at self-broadening is much more intense than in the case of air pressure induced broadening, since in the latter case the χ-function decreases faster with the frequency than in the case of self-broadening.

2.2. Non-LTE continuum for air pressure induced broadening (standard atmosphere)

Figure 6 depicts a wide-range spectrum of non-LTE water vapor continuum under conditions of standard atmosphere (in this case broadening by air – N_2 and O_2 – prevails).

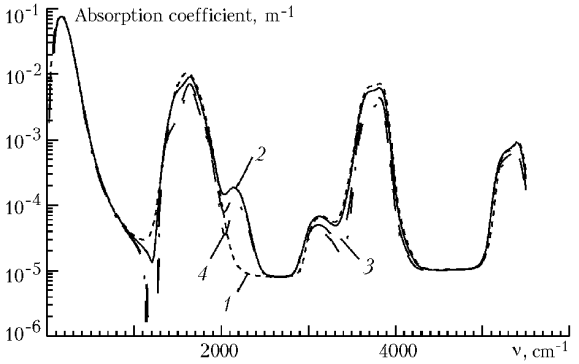

Fig. 6. Wide-range water vapor continuum spectrum under conditions of excitation of all H_2O levels with the same vibrational temperature T_V. Standard atmosphere: P = 1 atm, T = 288 K, $\tilde{N}_{H_2O} = 7.75 \cdot 10^3$ ppmV; T_V = 288 K (LTE) (*1*); 2000 (*2*); 5000 (*3*); 10000 K (*4*).

Calculation was conducted for conditions that all the H_2O levels gain the same vibrational temperature T_V as a result of excitation. The same T_V for all the levels assumes the Boltzmann distribution of vibrational population with the temperature T_V, and this makes impossible complete population inversion. In this case, only partial inversion is possible. As can be seen from Fig. 6, the shape of continuum markedly changes and differently in different spectral ranges: absorption may decrease, increase, or keep unchanged. The decrease of absorption in the central parts of rovibrational bands is explained by the mere increase in the population of the upper vibrational level in a transition, that is, decrease of the population difference (see, for example, the bands in the region of 1600, 3800, 5400 cm^{-1}).

The same factor causes marked (up to an order of magnitude) changes in absorption (first increase and then decrease) in the (010)–(020) and (010)–(100) hot bands lying in the region of 2000–2300 cm^{-1}. The drastic decrease in absorption (up to negative values) in the region of 1160–1280 cm^{-1} is a consequence of the effect of partial inversion at the transition (000)–(010) and, possibly, at the transition (010)–(020). The effect of partial inversion and negative absorption in H_2O was considered more thoroughly in Ref. 28. Figure 7 depicts the most interesting fragments on the expanded scale.

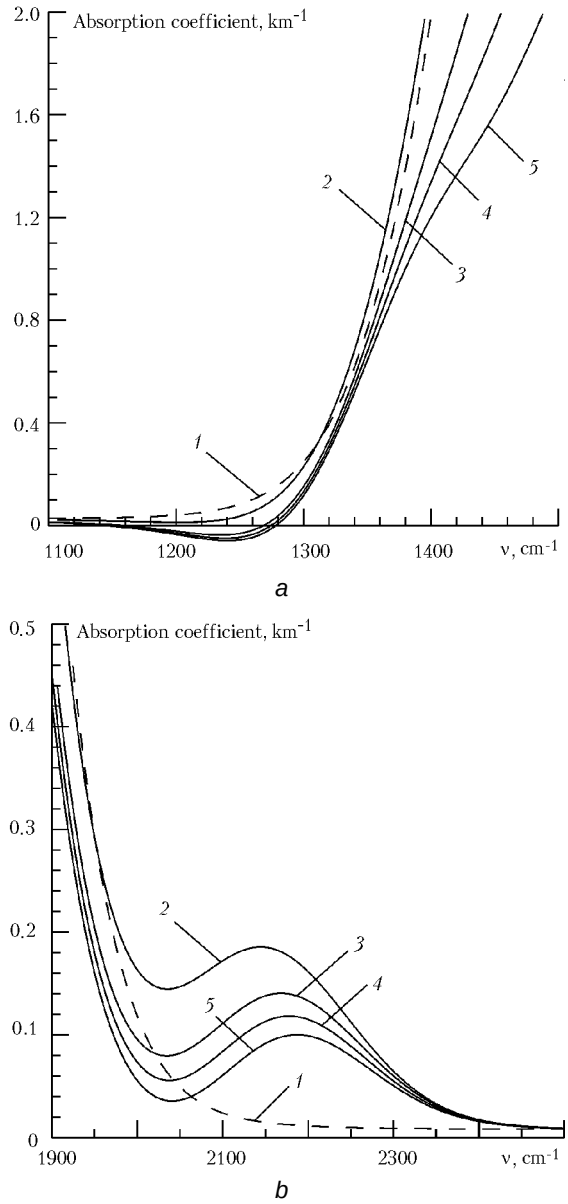

Fig. 7. Most interesting fragments of Fig. 6 (increased): region of the *P*-branch of the H_2O ν_2 band (*a*); region of the hot bands (010)–(001) and (010)–(100) (*b*): T_V = 288 K (equilibrium) (*1*); 2000 (*2*); 5000 (*3*); 10000 K (*4*).

The rotational band in the microwave region is almost not subject to the effect of vibrational excitation. This is quite natural since the decrease of absorption in the main rotational band (000)–(000) is compensated by the increase of absorption in the hot bands (010)–(010), (020)–(020) and others. It should be noted that the effect of partial inversion takes place also in the *P*-branches of the ν_1 and ν_3 bands, but it does not lead to negative absorption in the region of 3100–3500 cm^{-1} due to absorption in the $2\nu_2$ band. Selective excitation of vibrational levels (when $T_V \neq T_R$) for only one or a few levels,

all other levels being in equilibrium, leads to some extra interesting features connected with the possibility of appearing of full population inversion. Figure 8 depicts H_2O continuum in the same spectral intervals as in Fig. 7, but for the case of excitation of only (020), (100) and (001) levels.

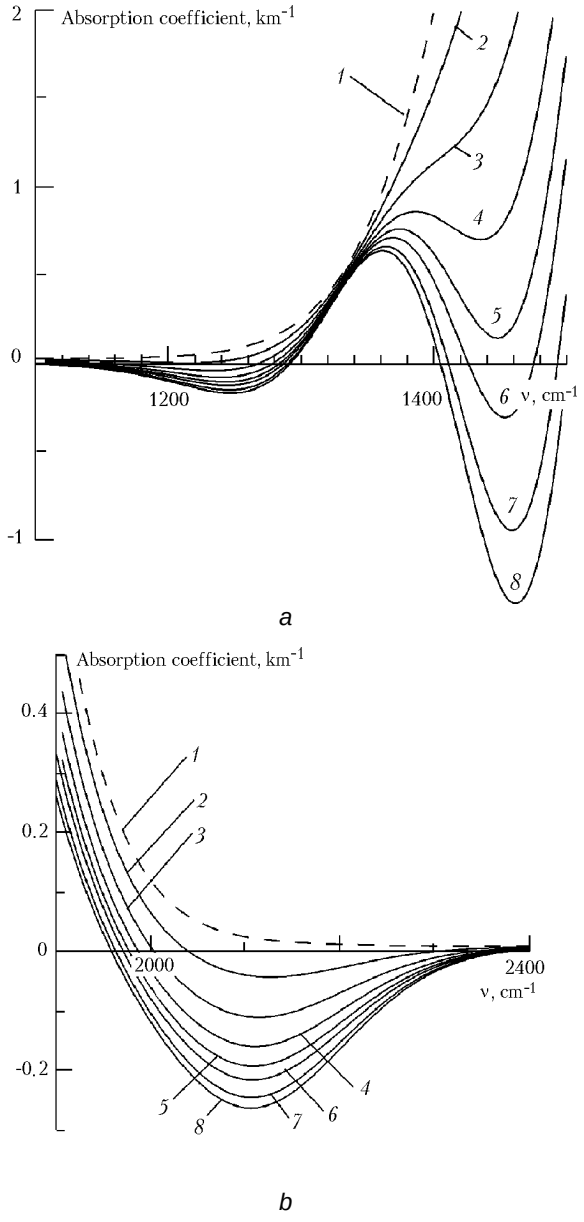

Fig. 8. Water vapor continuum under conditions of selective excitation of H_2O levels. Standard atmosphere: P = 1 atm, $\dot{O}$ = 288 K, $\tilde{N}_{H_2O}$ = $7.75 \cdot 10^3$ ppmV: only the level (020) is excited up to the vibrational temperature T_V (*a*); the levels (100) and (001) are excited up to the vibrational temperature T_V (*b*): T_V = 288 K (equilibrium) (*1*); 2000 (*2*); 3000 (*3*); 4000 (*4*); 5000 (*5*); 6000 (*6*); 8000 (*7*); 10000 K (*8*).

Such excitation leads to full inversion between the states mentioned above and the state (010), thus giving rise to strong negative absorption in the region of 1400–1500 cm^{-1} and somewhat weaker absorption in the region of 1950–2400 cm^{-1}. Negative absorption in the region 1160–1280 cm^{-1} caused by partial inversion turns out to be more evident, if only the level (020) is excited (cf. Fig. 7).

Evolution of non-LTE water vapor continuum is shown in Fig. 9. It is a very fast process at the atmospheric pressure. The relaxation rate is not constant: it is maximum in the beginning of the process and then decreases. Other features of spectroscopic manifestation of the relaxation process are connected with population of the state (010) during relaxation and, as a consequence, increase of absorption in the hot bands (010)–(001) and (010)–(100) and decrease of absorption in the (000)–(010) band.

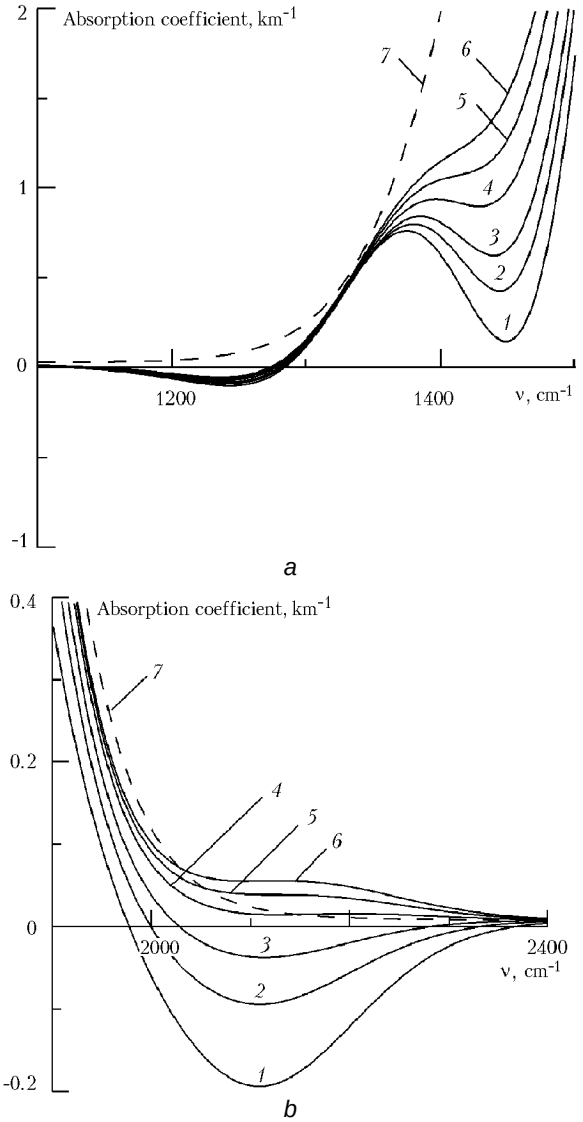

Fig. 9. Evolution of non-LTE water vapor continuum after instantaneous excitation of selected states. Standard atmosphere: P = 1 atm, $\dot{O}$ = 288 K, $\tilde{N}_{H_2O}$ = $7.75 \cdot 10^3$ ppmV: only the level (020) is excited up to T_V = 5000 K (*a*); the levels (100) and (001) are excited up to T_V = 5000 K (*b*): t = 0 (*1*), 1 (*2*), 2 (*3*), 4 (*4*), 6 (*5*), 8 ns (*6*), ∞ (*7*); T_V = $\dot{O}$ = 288 K (equilibrium).

2.3. Non-LTE continuum at self-broadening

As was noted above, the case of H_2O self-broadening is more efficient than air pressure induced broadening, and, consequently, continuum absorption of pure water vapor is higher than that of a mixture with the same H_2O partial pressure. Non-LTE continuum of pure water vapor is shown in Fig. 10.

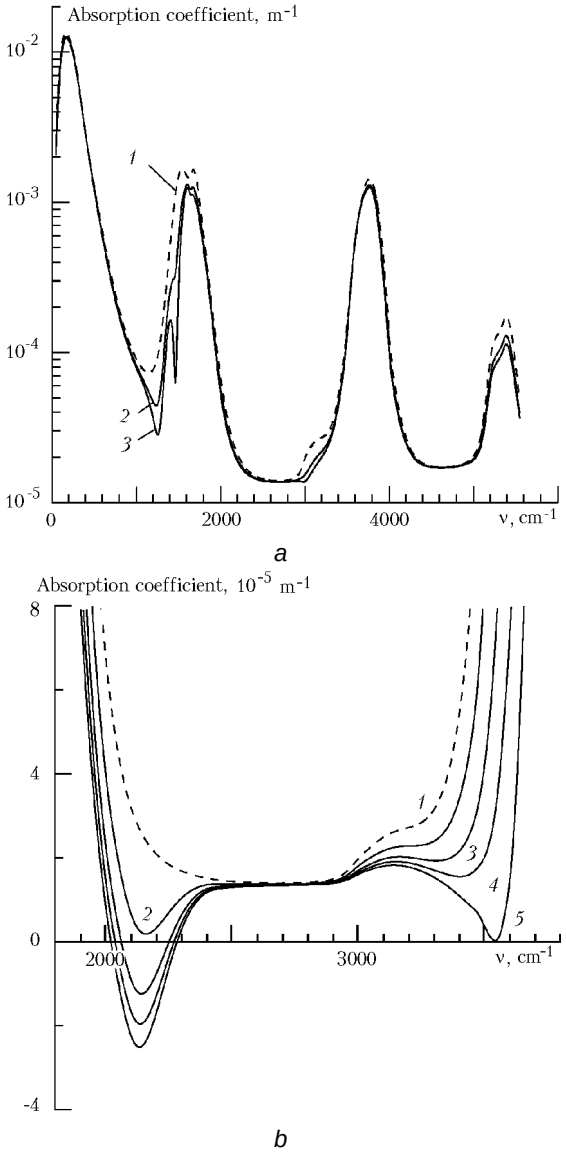

Fig. 10. Non-LTE continuum of pure water vapor at P_{H_2O} = 10 Torr. Excitation of selected levels: only the level (020) is excited up to the vibrational temperature T_V (*a*): T_V = 296 K (equilibrium) (*1*); 5000 (*2*); 10000 K (*3*); the levels (100) and (001) are excited up to T_V (*b*): T_V = 296 K (equilibrium) (*1*); 3000 (*2*); 5000 (*3*); 7000 (*4*); 10000 K (*5*).

It can be seen that the decrease of absorption in the case of excitation of selected levels is far more weaker than in the case of air pressure induced broadening (cf. Fig. 8). It is important that when the level (020) is excited, no negative absorption arises. The effect of negative absorption in the region of 2150 cm^{-1} proves to be an order of magnitude less than in the case of air pressure induced broadening (see Fig. 8).

It is interesting to follow the effect of the mixture composition on the spectrum of non-LTE water vapor continuum. The results of calculations for the case of excitation of the (020) level at different H_2O partial pressures for the pure vapor and for humid air at the total pressure of 1 atm are shown in Fig. 11.

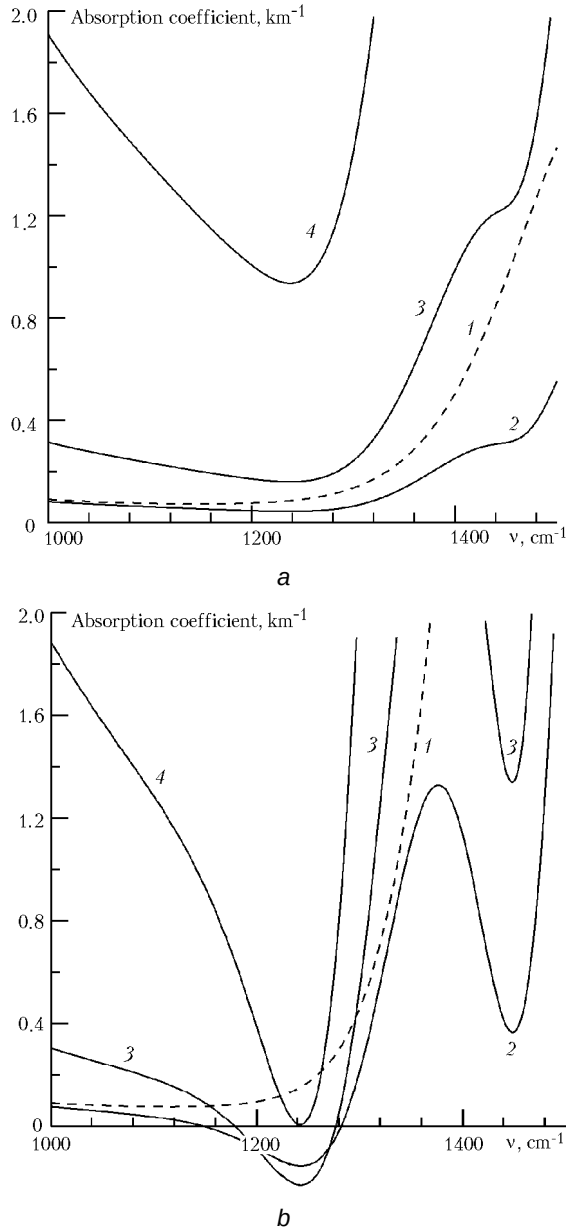

Fig. 11. Effect of the gas composition and H_2O partial pressure on the spectrum of non-LTE continuum. The region of the *Ð*-branch of the Í$_2$Î ν_2 band. Excitation of the level (020) up to T_V = 5000 K: pure water vapor (*a*); water vapor + air at the total pressure of 760 Torr, T = 296 K: P_{H_2O} = 10 Torr at T_V = 296 K (equilibrium) (*1*); 10 (*2*); 20 (*3*); 50 Torr (*4*).

Figure 12 depicts the dependence of non-LTE continuum absorption of humid air on the H_2O partial pressure calculated at some frequencies. From Figs. 11 and 12 we can draw the following conclusion: non-LTE continuum strongly and differently depends on the mixture composition at different frequencies.

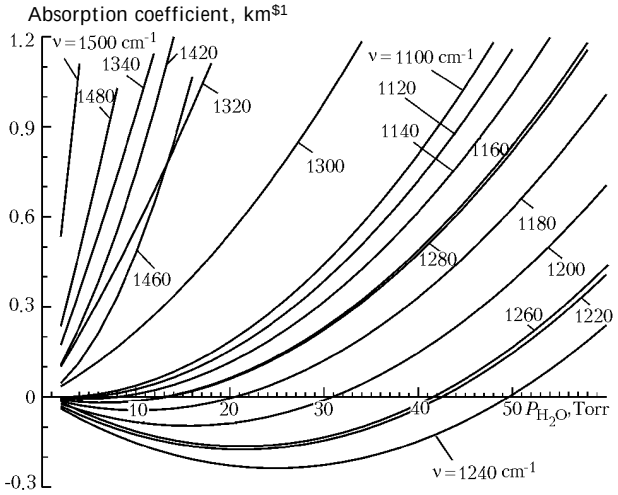

Fig. 12. Dependence of non-LTE continuum of humid air at some frequencies on the H_2O partial pressure. Excitation of the (020) level up to T_V = 5000 K. Total H_2O + air pressure is 1 atm. T = 296 K. Frequencies (in cm^{-1}) are indicated nearby the curves.

3. Idea of experiments of the pumping–sensing type for modifying the semiempirical χ-functions and revealing the nature of water vapor continuum

The results obtained open extra possibilities for studying water vapor absorption continuum that are unavailable in equilibrium spectroscopy. For example, experiments of the pumping–sensing type in water vapor can be proposed. To pump H_2O levels, pico- or femtosecond lasers can be used,[35,36] and variations of weak absorption can be sounded with the use of new spectroscopic techniques (for example, intracavity spectroscopy, cavity ringdown spectroscopy, etc.[37,38]). If we excite (pump) a selected H_2O state by a short laser pulse and then have a quick record of the non-LTE IR spectrum in the regions corresponding to absorption bands attributed to the excited state, we can find suitable χ_k-functions for these bands using the least squares method. It is clear that only the use of experimentally obtained χ_k-function corresponding to every band will allow reliable prediction of the properties of non-LTE continuum. Note that this modification of the approach of semiempirical correction χ-function for description of continuum (that is, introduction of more than one χ_k-functions) makes even the CKD equilibrium technique more flexible, for example, in the case of its application to the cases with high temperatures.

Experiments of the pumping–sensing type in water vapor can help us to reveal the nature of continuum, giving the answer to the question: is it due to absorption by dimers or monomers? These experiments are based on a significant difference in the rotational structure of absorption bands of water monomer H_2O and dimer $(H_2O)_2$. When we pump vibrational states of the monomer in its bending mode ν_2, we obtain the effect of full and partial inversion and, as a consequence, significant decrease of absorption (down to negative values) in the region of 1100–1600 cm^{-1} (see Figs. 7 and 8 for air pressure induced broadening and Fig. 10 for self-broadening). Recall that the decrease of absorption in the region of 1200 cm^{-1} is caused by the effect of partial inversion. It is quite natural that pumping the states of the monomer ν_2 mode we also excite the corresponding intramolecular vibrations of the dimer (since they are shifted only a little bit with respect to the monomer). This should seemingly lead to the same effects of inversion and decrease of absorption. However, it is true only for the effect of full inversion, but not for the case of partial inversion.

In Ref. 28 it was shown that the effect of partial inversion is pronounced in spectra of asymmetric-top molecules, while for symmetric-top molecules it is much weaker. The water monomer in its ground state is a typical asymmetric-top molecule (its rotational constants are strongly different: A = 27.8807 cm^{-1}, B = 14.5217 cm^{-1}, C = 9.2775 cm^{-1} [Refs. 39 and 40]). On the other hand, the water dimer in the ground state is an oblong almost symmetric top (its rotational constants are A = 6.3442 cm^{-1}, B = 0.2059 cm^{-1}, C = 0.2049 cm^{-1} [Ref. 41]). Thus it is clear that the effect of partial inversion will be less pronounced in the water dimer as compared to the monomer. Consequently, if in the experiments on excitation of the water vapor ν_2 mode we will observe the considerable decrease of absorption in the region of 1200 cm^{-1}, then it will be the indication of the monomer nature of continuum in this region.

Conclusions

1. The CKD model of water vapor continuum has been extended to nonequilibrium vibrational conditions.

2. It has been found that the spectrum of non-LTE continuum strongly depends (both qualitatively and quantitatively) on the population of H_2O levels and the water vapor partial pressure in a mixture. The effects of strong increase and decrease (down to negative values) of H_2O continuum absorption under non-LTE conditions have been obtained.

3. A method has been proposed to improve the quality of continuum description with the use of semiempirical χ-function for the line shape of the water monomer. The method involves recording of nonequilibrium IR absorption spectra of water vapor

in various bands and determining several χ_k-functions characterizing every band separately in place of one χ-function identical for all the bands (as is the case in the classical CKD method).

4. It has been proposed to conduct pumping–sensing experiments in order to reveal the nature of water vapor continuum (dimer / monomer). The idea of these experiments is based on different degree of manifestation of the partial population inversion effect in the spectrum of the ν_2 band of the monomer H_2O and dimer $(H_2O)_2$ in the region of 1200 cm^{-1}.

References

1. L.I. Nesmelova, S.D. Tvorogov, and V.V. Fomin, *Spectroscopy of Line Wings* (Nauka, Novosibirsk, 1977), 144 pp.
2. S.A. Clough, F.X. Kneizys, R. Davies, R. Gamache, and R. Tipping, in: *Atmospheric Water Vapor*, ed. by A. Deepak, T.D. Wilkerson, and L.H. Ruhnke (Academic Press, New York, 1980), pp. 25–46.
3. S.A. Clough, F.X. Kneizys, and R.W. Davies, Atmos. Res. **23**, 229–241 (1989).
4. Q. Ma and R.H. Tipping, J. Chem. Phys. **93**, No. 9, 6127–6139 (1990).
5. Q. Ma and R.H. Tipping, J. Chem. Phys. **95**, No. 9, 6290–6301 (1991).
6. S.D. Tvorogov, Atmos. Oceanic Opt. **8**, Nos. 1–2, 7–13 (1995).
7. V.N. Aref'ev and V.I. Dianov-Klokov, Opt. Spektrosk. **42**, No. 5, 849–855 (1977).
8. V.I. Dianov-Klokov and V.M. Ivanov, Izv. Akad. Nauk SSSR, Ser. Fiz. Atmos. Okeana **17**, No. 6, 587–593 (1981).
9. R.E. Roberts, J.E.A. Selby, and L.M. Biberman, Appl. Opt. **15**, No. 9, 2085–2090 (1976).
10. S.H. Suck, J.L. Kassner, and Y. Yamaguchi, Appl. Opt. **18**, No. 15, 2609–2618 (1979).
11. Yu.S. Demchuk, S.O. Mirumyants, N.I. Moskalenko, and V.L. Filippov, Opt. Spektrosk. **69**, No. 1, 64–70 (1990).
12. Yu.S. Demchuk, S.O. Mirumyants, and S.L. Vinokurov, Opt. Spektrosk. **72**, No. 1, 93–97 (1992).
13. V.F. Golovko, J. Quant. Spectrosc. Radiat. Transfer **65**, 621–644 (2000).
14. V.F. Golovko, J. Quant. Spectrosc. Radiat. Transfer **69**, 431–446 (2001).
15. H.R. Carlon, Infrared Phys. **19**, No. 3, 549–557 (1979).
16. S.H. Suck, J.L. Kassner, R.E. Thurman, P.S. Yue, and R.A. Anderson, J. Atmos. Sci. **38**, No. 6, 1272–1278 (1981).
17. V.I. Dianov-Klokov and V.M. Ivanov, Izv. Akad. Nauk SSSR, Ser. Fiz. Atmos. Okeana **14**, No. 3, 328–330 (1978).
18. N.N. Shchelkanov, Atmos. Oceanic Opt. **9**, No. 7, 565–568 (1996).
19. M.E. Thomas, Proc. SPIE **2471**, 66–76 (1995).
20. S.S. Penner, *Quantitative Molecular Spectroscopy and Gas Emissivities* (Addison-Wesley, Reading, MA, 1959), 587 pp.
21. S.A. Losev, *Gas Dynamic Lasers* (Nauka, Moscow, 1977).
22. B.F. Gordiets, A.I. Osipov, and L.A. Shelepin, *Kinetic Processes in Gases and Molecular Lasers* (Nauka, Moscow, 1980), 512 pp.
23. M.K. Bullitt, P.M. Bakshi, R.H. Picard, and R.D. Sharma, J. Quant. Spectrosc. Radiat. Transfer **34**, No. 1, 33–53 (1985).
24. R.O. Manuilova and G.M. Shved, J. Atmos. Terr. Phys. **54**, No. 9, 1149–1168 (1992).
25. D.P. Edwards and M. Lopez-Puertas, J. Geophys. Res. D **98**, No. 8, 14955–14977 (1993).
26. S.V. Ivanov, O.G. Buzykin, and D.A. Rusyanov, Proc. SPIE **3688**, 501–507 (1999).
27. S.V. Ivanov, O.G. Buzykin, and D.A. Rusyanov, Proc. SPIE **3732**, 157–163 (1999).
28. O.G. Buzykin and S.V. Ivanov, Opt. Spektrosk. **88**, No. 5, 772–781 (2000).
29. W.S. Benedict, M.A. Pollack, and W.J. Tomlinson III, IEEE J. Quantum Electron. **QE-5**, No. 2, 108–124 (1969).
30. D.E. Burch, *Continuum Absorption by* H_2O. Rep. AFGL-TR-81-0300 (U.S. Air Force Geophys. Laboratory, Hanscom Air Force Base, Mass., 1981).
31. D.E. Burch, *Absorption by* H_2O *in Narrow Windows between* 3000–4200 cm^{-1}. Rep. AFGL-TR-85-0036 (U.S. Air Force Geophys. Laboratory, Hanscom Air Force Base, Mass., 1985).
32. D.E. Burch and R.L. Alt, *Continuum Absorption in the* 700–1200 cm^{-1} *and* 2400–2800 cm^{-1} *Windows*. Rep. AFGL-TR-84-0128 (U.S. Air Force Geophys. Laboratory, Hanscom Air Force Base, Mass., 1984).
33. L.S. Rothman, C.P. Rinsland, A. Goldman, S.T. Massie, D.P. Edwards, J.-M. Flaud, A. Perrin, C. Camy-Peyret, V. Dana, J.-Y. Mandin, J. Schroeder, A. McCann, R.R. Gamache, R.B. Wattson, K. Yoshino, K.V. Chance, K.W. Jucks, L.R. Brown, V. Nemtchinov, and P. Varanasi, J. Quant. Spectrosc. Radiat. Transfer **60**, No. 5, 665–710 (1998).
34. O.G. Buzykin, A.A. Ionin, S.V. Ivanov, A.A. Kotkov, L.V. Seleznev, and A.V. Shustov, Laser and Particle Beams **18**, 697–713 (2000).
35. Z.E. Dolya, N.B. Nazarova, G.K. Paramonov, and V.A. Savva, Opt. Spektrosk. **65**, No. 6, 1242–1247 (1988).
36. G.K. Paramonov, Opt. Spektrosk. **70**, No. 2, 446–452 (1991).
37. A.D. Bykov, L.N. Sinitsa, and V.I. Starikov, *Experimental and Theoretical Methods in Spectroscopy of Water Vapor Molecules* (SB RAS Publishing House, Novosibirsk, 1999), 376 pp.
38. J.G. Cormier, R. Ciurylo, and J.R. Drummond, J. Chem. Phys. **116**, No. 3, 1030–1034 (2002).
39. C. Camy-Peyret and J.-M. Flaud, Mol. Phys. **32**, No. 2, 523–537 (1976).
40. A.D. Bykov, Yu.S. Makushkin, and O.N. Ulenikov, *Vibrational-Rotational Spectroscopy of Water Vapor* (Nauka, Novosibirsk, 1989), 296 pp.
41. L.H. Coudert and J.T. Hougen, J. Mol. Spectrosc. **139**, 259–277 (1990).